DYNAMIC RESPONSE OF STRAINED PREMIXED FLAMES TO EQUIVALENCE RATIO GRADIENTS

Y. M. MARZOUK,[1] A. F. GHONIEM[1] AND H. N. NAJM[2]

[1]Department of Mechanical Engineering
Massachusetts Institute of Technology
Cambridge, MA 02139, USA
[2]Combustion Research Facility
Sandia National Laboratories
Livermore, CA 94551, USA

Premixed flames encounter gradients of mixture equivalence ratio in stratified charge engines, lean premixed gas-turbine engines, and a variety of other applications. In cases for which the scales—spatial or temporal—of fuel concentration gradients in the reactants are comparable to flame scales, changes in burning rate, flammability limits, and flame structure have been observed. This paper uses an unsteady strained flame in the stagnation point configuration to examine the effect of temporal gradients on combustion in a premixed methane/air mixture. An inexact Newton backtracking method, coupled with a preconditioned Krylov subspace iterative solver, was used to improve the efficiency of the numerical solution and expand its domain of convergence in the presence of detailed chemistry.

Results indicate that equivalence ratio variations with timescales lower than 10 ms have significant effects on the burning process, including reaction zone broadening, burning rate enhancement, and extension of the flammability limit toward leaner mixtures. While the temperature of a flame processing a stoichiometric-to-lean equivalence ratio gradient decreased slightly within the front side of the reaction zone, radical concentrations remained elevated over the entire flame structure. These characteristics are linked to a feature reminiscent of "back-supported" flames—flames in which a stream of products resulting from burning at higher equivalence ratio is continuously supplied to lower equivalence ratio reactants. The relevant feature is the establishment of a positive temperature gradient on the products side of the flame which maintains the temperature high enough and the radical concentration sufficient to sustain combustion there. Unsteadiness in equivalence ratio produces similar gradients within the flame structure, thus compensating for the change in temperature at the leading edge of the reaction zone and accounting for an observed "flame inertia." For sufficiently large equivalence ratio gradients, a flame starting in a stoichiometric mixture can burn through a very lean one by taking advantage of this mechanism.

Introduction

Premixed flames encounter equivalence ratio gradients in many applications. Important examples include stratified charge, spark-ignition engines [1,2] and lean premixed gas-turbine combustors [3,4]. In the former, a small volume of the total mixture is made rich close to the spark plug, to guarantee ignition and help sustain flame propagation in the leaner bulk of the mixture. In the latter, pressure oscillations arising from coupling between the acoustic field and the combustion zone can lead to oscillations in air mass flow rate near the fuel injectors, producing oscillations in equivalence ratio at the flame. Moreover, pulsed fuel injection may be used to impose similar oscillations in mixture composition to suppress combustion instabilities resulting from alternate mechanisms. In yet other applications for which burning occurs through nominally premixed reactants, a flame can still encounter pockets of richer or leaner mixture produced by inhomogeneous mixing, and thus propagate through gradients in fuel concentration.

In all the cases described above, when the turbulence intensity is moderate, the combustion process can be modeled as a wrinkled laminar flame in which burning occurs across a strained laminar flame surface. This paper examines the impact of equivalence ratio variations on the structure and burning rate of such a strained flame.

Order-of-magnitude arguments can be used to quantify single, dominant gradients in the equivalence ratio ϕ for many of the applications mentioned. In the case of combustion instability, oscillation frequencies are typically $O(500–1000 \text{ Hz})$, and hence the timescale of ϕ variation is approximately 1–2 ms. In a spark-ignition engine, the total combustion time is $O(3 \text{ ms})$, a small fraction of which is taken for the transition between the stoichiometric mixture near the spark plug to the leaner mixture in

Report Documentation Page

Public reporting burden for the collection of information is estimated to average 1 hour per response, including the time for reviewing instructions, searching existing data sources, gathering and maintaining the data needed, and completing and reviewing the collection of information. Send comments regarding this burden estimate or any other aspect of this collection of information, including suggestions for reducing this burden, to Washington Headquarters Services, Directorate for Information Operations and Reports, 1215 Jefferson Davis Highway, Suite 1204, Arlington VA 22202-4302. Respondents should be aware that notwithstanding any other provision of law, no person shall be subject to a penalty for failing to comply with a collection of information if it does not display a currently valid OMB control number.

1. REPORT DATE 04 AUG 2000	2. REPORT TYPE N/A	3. DATES COVERED -

4. TITLE AND SUBTITLE	5a. CONTRACT NUMBER
Dynamic Response of Strained Premixed Flames to Equivalence Ratio Gradients	5b. GRANT NUMBER
	5c. PROGRAM ELEMENT NUMBER
6. AUTHOR(S)	5d. PROJECT NUMBER
	5e. TASK NUMBER
	5f. WORK UNIT NUMBER

7. PERFORMING ORGANIZATION NAME(S) AND ADDRESS(ES) **Department of Mechanical Engineering Massachusetts Institute of Technology Cambridge, MA 02139, USA**	8. PERFORMING ORGANIZATION REPORT NUMBER

9. SPONSORING/MONITORING AGENCY NAME(S) AND ADDRESS(ES)	10. SPONSOR/MONITOR'S ACRONYM(S)
	11. SPONSOR/MONITOR'S REPORT NUMBER(S)

12. DISTRIBUTION/AVAILABILITY STATEMENT
Approved for public release, distribution unlimited

13. SUPPLEMENTARY NOTES
See also ADM001790, Proceedings of the Combustion Institute, Volume 28. Held in Edinburgh, Scotland on 30 July-4 August 2000.

14. ABSTRACT

15. SUBJECT TERMS

16. SECURITY CLASSIFICATION OF:			17. LIMITATION OF ABSTRACT	18. NUMBER OF PAGES	19a. NAME OF RESPONSIBLE PERSON
a. REPORT **unclassified**	b. ABSTRACT **unclassified**	c. THIS PAGE **unclassified**	**UU**	**8**	

the bulk of the cylinder volume. Under these circumstances, the following questions arise: When the timescales of ϕ variation are of the order of magnitude of the nominal flame timescales, will the flames respond in a quasi-steady fashion; that is, will they adjust almost instantaneously to the imposed strain, or will some "flame inertia" affect propagation into the leaner mixture? Will adjustment to different values of ϕ introduce changes to the flame structure that have a significant impact on the burning rate and species distributions? And can the presence of these gradients explain the experimentally observed extension of flammability limits into leaner mixtures [1,5]?

In this paper, we answer these questions using an unsteady, strained flame code recently developed [6,7]. Because the code considers a flame stabilized in a stagnation-point flow, imposed variations in ϕ are modeled as temporal gradients; these can be rendered equivalent to spatial gradients by a Lagrangian transformation.

Formulation and Numerical Solution

The impact of variable ϕ on burning under finite strain was modeled with an axisymmetric stagnation-point flame configuration, in which a reactants stream impinged on a stream of burned combustion products. This formulation has been thoroughly discussed elsewhere [8–11], so only an outline is presented here. One-dimensional governing equations were obtained by applying a boundary layer approximation across the flame and solving along the stagnation streamline $x = 0$; here, y was the coordinate normal to the flame surface. Letting the imposed strain rate ε define the outer flow on the reactants side, $u_\infty = \varepsilon x$, $v_\infty = -\varepsilon y$, and introducing the notation $U \equiv u/u_\infty$, $V \equiv \rho v$, we obtained the following equations for species, energy, momentum, and mass conservation, respectively:

$$\rho \frac{\partial Y_k}{\partial t} + V \frac{\partial Y_k}{\partial y} - \frac{\partial}{\partial y}\left(\rho D_k \frac{\partial Y_k}{\partial y}\right)$$
$$- \dot{w}_k W_k = 0 \qquad (1)$$

$$\rho \frac{\partial T}{\partial t} + V \frac{\partial T}{\partial y} - \frac{1}{c_p}\frac{\partial}{\partial y}\left(\lambda \frac{\partial T}{\partial y}\right)$$
$$- \sum_k \frac{\dot{w}_k h_k}{c_p} = 0 \qquad (2)$$

$$\rho \frac{\partial U}{\partial t} + \rho U \frac{1}{\varepsilon}\frac{\partial \varepsilon}{\partial t} + \rho U^2 \varepsilon + V \frac{\partial U}{\partial y}$$
$$- \frac{\partial}{\partial y}\left(\mu \frac{\partial U}{\partial y}\right) - \rho_u\left(\frac{1}{\varepsilon}\frac{\partial \varepsilon}{\partial t} + \varepsilon\right) = 0 \qquad (3)$$

$$\frac{\partial \rho}{\partial t} + \frac{\partial V}{\partial y} + 2\rho U \varepsilon = 0 \qquad (4)$$

Here Y_k is the mass fraction of species k, while D_k is the corresponding mixture-averaged diffusion coefficient and W_k and $\dot{w}_k$ are the molar weight and molar production rate, respectively. In the remaining equations, c_p is the mixture specific heat, λ is the thermal conductivity, h_k is the molar enthalpy, ρ_u is the density of the reactants mixture, and μ is the dynamic viscosity of the mixture. The enthalpy flux term was neglected in the energy equation while thermal diffusion velocity was neglected in each species transport equation. Smooke [12] and others have shown that both effects are unimportant to the laminar strained flame.

In the ensuing analysis, strain rate was held constant. Unsteadiness entered in the form of the species and temperature boundary conditions at $\pm\infty$; these conditions define the composition and temperature of the two incoming streams of the stagnation-point flow.

$$y = \pm\infty: Y_k = Y_{k,\pm\infty}(t), \ T = T_{\pm\infty}(t) \qquad (5)$$

The continuity equation required only one boundary condition, which specified zero velocity at the stagnation point, $V(y = 0) = 0$. The momentum conservation equation required two boundary conditions: At an unburned stream, $u = u_\infty$, so the boundary condition is by definition $U = 1$. Setting the spatial gradients in equation 3 to zero gives the boundary condition on the burned stream; for steady strain, it becomes $U_b = \sqrt{\rho_u/\rho_b}$, where ρ_b is the density of the burned mixture.

To accurately characterize flame structure and response, detailed transport and chemistry were used to evaluate transport coefficients and reaction terms in the model. Following the approach validated in Ref. [12], a fixed Lewis number Le_k was chosen for each species, constant across the flame. The Prandtl number was chosen constant and equal to 0.75, while a curve fit was used to calculate the ratio λ/c_p. We used a $C_{(1)}$ kinetic model for methane/air combustion given in Ref. [13], consisting of 46 reactions among 16 species.

Numerical solution of the governing equations was obtained via a fully implicit finite difference method, as necessitated by the stiffness of detailed kinetics. A first-order backward Euler formulation was used; a first-order upwind discretization was applied to convective terms, while diffusion terms were discretized to second-order accuracy. These spatial discretizations were performed on a non-uniform adaptive grid, permitting a dynamic clustering of meshpoints in regions where spatial gradients were strong. We enforced a limit on the maximum change between neighboring meshpoints for all dependent variables (T, U, V, Y_k, $\dot{w}_k$) and their gradients, thus ensuring that the reaction zone of each species was resolved throughout the integration time. Using these criteria, for the present mechanism, the minimum grid scale was $O(10\ \mu m)$.
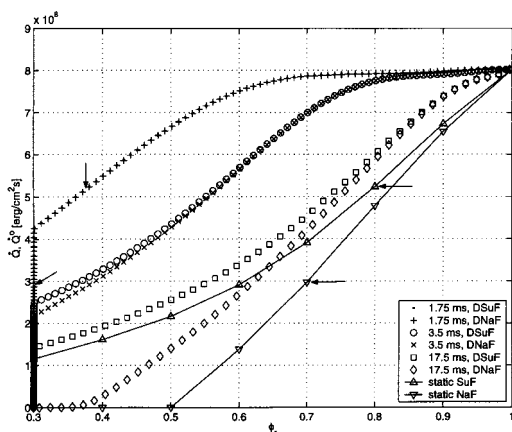
FIG. 1. Heat release rates for static and dynamic flames, as a function of instantaneous reactants-side equivalence ratio, ϕ_r. Arrows denote cases shown in Figs. 4, 6, and 8.

At each time step, discretization reduced the governing equations to a set of nonlinear algebraic equations. We implemented a novel set of numerical methods to solve these equations efficiently and robustly [6]. An inexact Newton iteration [14] converged to the solution of the nonlinear equations but avoided precisely solving the Newton condition far away from a solution, when the linear model of Newton's method may be poor. This inexact Newton method was coupled with a backtracking globalization to improve its domain of convergence [15]. Solution of the linear system at each Newton iteration proceeded via a Krylov subspace method, BiCGSTAB (BiConjugate Gradients Stabilized) [16,17]. Because detailed chemistry renders this linear system ill-conditioned, BiCGSTAB must be accelerated with an incomplete LU factorization preconditioner [17].

Results

The unsteady strained flame model described above was used to examine the impact of ϕ variation on burning rate, flame structure, and extinction. Since the temperature and species mass fraction boundary conditions of the formulation were arbitrarily adjustable, numerous schemes for imposing mixture variation on the flame were possible. We used ϕ_r to denote the equivalence ratio of the reactants, injected at $y = -\infty$, with the temperature of the reactants mixture always 300 K. The composition and temperature of the products stream, however, corresponded to the chemical equilibrium state of a mixture with equivalence ratio ϕ_b under adiabatic, constant-pressure conditions.

Static Flames with and without Back Support

We began with a comparison of two steady-state flames, one with $\phi_r = \phi_b$ and the other with ϕ_b constant at 1.0. The first flame was labeled the NaF (for *natural flame*) and the second the SuF (for *supported flame*). The objective of this comparison was to determine, in the absence of time-dependent effects, the impact that products of a high-ϕ mixture may have on the burning of a leaner mixture. Specifically, we wished to examine the mechanism by which the high-ϕ_b products mixture could accelerate the burning of a lean mixture with ϕ_r above the flammability limit or sustain burning in a lean mixture with ϕ_r below the flammability limit.

Figure 1 shows the dependence of the integrated heat release rate $\dot{Q}$ on ϕ_r for a number of strained flames. All flames discussed in this paper were subject to a constant strain rate of 300 s^{-1}. Here we focus on the static flames of Fig. 1, marked with triangles. The static simulations give rise to the following observations:

- For all values of ϕ_r, the SuF exhibits a higher heat release rate than the NaF, with the difference increasing dramatically as the mixtures becomes leaner.
- While the NaF is extinguished by $\phi_r = 0.5$, the SuF continues to burn down to the lowest equivalence ratio examined.

The experimental results of Ref. [5] support the second observation: no matter how low the equivalence ratio of propane/air reactants, a shear layer between a reactants stream and a products stream maintained at 1770 K showed a finite rate of heat release. Ra [1] found that it was not possible to initiate a flame in a stationary propane/air mixture with $\phi < 0.55$ using a laser-ignition source in experiments, or with $\phi < 0.4$ using a heat source in numerical simulations. However, igniting a small bubble of stoichiometric mixture did sustain burning for some time in a mixture with ϕ slightly below 0.5 in the experiments, and for even lower values of ϕ in numerical simulations.

To examine the reasons for enhanced or sustained burning in the SuF, Fig. 2 shows profiles of temperature, OH mass fraction and diffusion flux, and the source term in the energy equation, $\dot{w}_T \equiv \Sigma_k \dot{w}_k h_k$, for the NaF and the SuF at $\phi_r = 0.6$. Several interesting observations can be made here:

- While the temperature at the peak burn rate is almost the same for both flames, $\dot{w}_T$ is much higher in the SuF than in the NaF.
- The tail of $\dot{w}_T$ on the burned side of the SuF is longer than that of the NaF; that is, burning is sustained further on the products side of SuF, contributing to the enhancement in $\dot{Q}$.
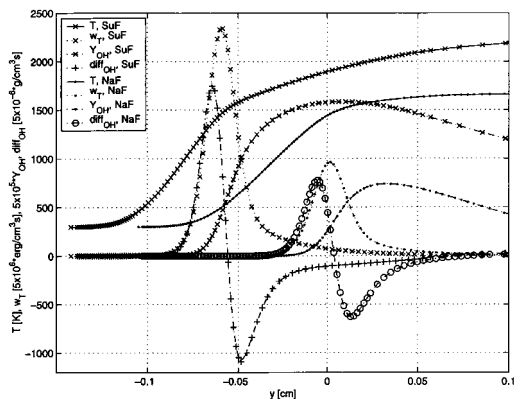- As the burning rate of a stagnation-point flame decreases, the reaction zone tends to stabilize itself

FIG. 2. Supported flame and natural flame structures, static at $\phi_r = 0.6$, showing T, $\dot{w}_T$, Y_{OH}, and net diffusion of OH.
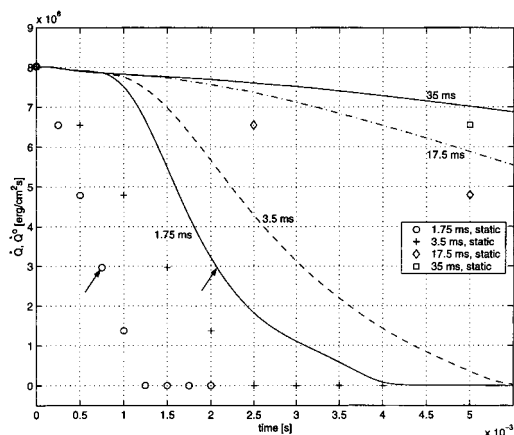

FIG. 3. $\dot{Q}$ versus time for natural flames subject to various $d\phi/dt$. Lines are dynamic behavior, while the symbols are static $\dot{Q}$ corresponding to the instantaneously imposed ϕ. Arrows denote cases shown in Figs. 4 and 6.

closer to the stagnation plane. Indeed, in the illustrated case of $\phi_r = 0.6$, the reaction zone of the NaF straddles the stagnation point while the SuF is stabilized well into the reactants stream.

Since the reaction zone temperatures of the two flames were nearly equal, a strong contribution to the difference in reaction rates must be the higher concentration of radicals in the reaction zone of the SuF—for OH, nearly twice that of the NaF. Both temperature and radical concentrations imposed at the products-side boundary condition were higher in the SuF than in the NaF, thus maintaining higher values throughout the products side, with radical concentrations increasing further to the right of the reaction zone. The result was a stronger net diffusive

flux of OH into the reaction zone of the SuF, as seen in Fig. 2. Similar results were observed for the radicals O and H.

As ϕ_r falls below 0.6, the SuF continues to burn while extinction is observed in the NaF. This precipitous decline in reaction rates coincides with the reaction zone of the NaF crossing the stagnation plane into regions of high products concentration. While the temperature in the reaction zone remains high, fuel, oxidizer, and radical concentrations drop due to the presence of products, leading to a falloff of all reaction rates [18]. Simultaneously, convection reverses sign and counteracts diffusion, driving reactants away from the reaction zone and toward the stagnation plane.

Static versus Dynamic Natural Flames

To examine the impact of ϕ variation on heat release rate and flame structure, we turned to cases in which ϕ_r varies linearly in time. For these cases, ϕ_r immediately ahead of the flame was reduced from 1.0 to 0.3 over four distinct time spans: 1.75 ms, 3.5 ms, 17.5 ms, and 35 ms. Here, "ahead of the flame" is defined as the leading edge of the temperature profile, the point at which the temperature gradient rises to a small finite threshold.

Definition of the mixture boundary conditions on the burned side of the flame is more subtle, for as a strained flame propagates through an equivalence ratio gradient, the state of the products left in the wake of the flame may change continuously. To model this case using the stagnation-point flame code, we note that the mixture takes essentially a flame timescale to burn through the flame structure, that is, to reach the products side. Therefore, if the conditions on the burned side are determined by the combustion of the reactants as they move through the flame, and if the reactants state changes continuously, conditions on the burned side must be delayed from conditions on the reactants side by a flame timescale. Thus, we assumed that $\phi_b = \phi_r(t - \tau_f)$ and updated both continuously, taking a nominal flame time scale τ_f to be 1 ms. A flame using this scheme for defining boundary conditions was labeled a DNaF (*Dynamic Natural Flame*).

To assess the impact of ϕ_r variation, we compared heat release rates for these dynamic flames with those obtained for static flames, shown as functions of time in Fig. 3. Static heat release rates correspond to a NaF burning a steady reactants stream whose ϕ_r is the same as the instantaneous ϕ_r ahead of the dynamic flame. The same comparison, plotted against the instantaneous value of ϕ_r, is shown in Fig 1. At the early stages, the burning rate lags behind the value corresponding to its current ϕ_r by about 1 ms. This is the flame timescale, the time it takes the reactants ahead of the flame to diffuse into the reaction zone and burn, suggesting that the observed
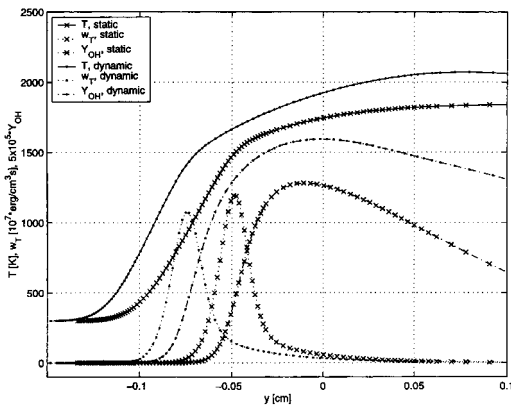
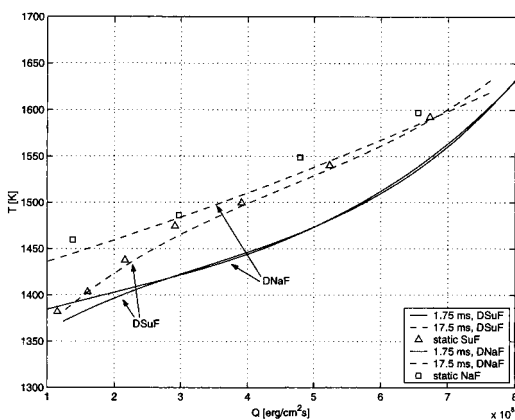FIG. 4. Comparison of dynamic and static natural flame structure at $\dot{Q} = 2.96 \times 10^8$ erg/(cm^2 s).

FIG. 5. T at max($\dot{w}_T$) versus $\dot{Q}$, dynamic and static flames.

time lag is due to the finite transport rate within the flame structure. (Note the distinction between the *delay time*, used to define the boundary condition on the DNaF, and the *time lag*, observed in flame response to imposed changes in ϕ.) The observed time lag increases as ϕ_r decreases since the flame becomes thicker as the mixture becomes leaner. Results in Figs. 1 and 3 indicate that

- the value of $\dot{Q}$ is always higher for the dynamic flame than for the static flame, since ϕ_r is decreasing.
- while the static flame tends to extinguish around $\phi_r = 0.5$, the dynamic flame continues to burn through lower values of ϕ_r.
- the higher $d\phi_r/dt$, the lower the equivalence ratio which can support burning; that is, there is a "flame inertia" whose effect becomes more pronounced with faster gradients in ϕ.

While the transport time lag can explain the higher burning rate of the DNaF, the interaction of finite transport rates and $d\phi_r/dt$ must have an effect on flame structure. In Fig. 4, we compare the temperature, OH concentration, and $\dot{w}_T$ profiles of a dynamic flame with those of a static flame that produces the same value of $\dot{Q}$. Both flames are marked with arrows in Figs. 1 and 3. The static flame corresponds to $\phi_r = 0.7$, and the dynamic flame corresponds to the 1.75 ms change in ϕ_r, probed 2.075 ms from the start of the calculations. The reason for choosing the two flames at the same value of $\dot{Q}$ is to remove the impact of time lag and different values of ϕ_r, and to focus instead on the effect of the ϕ gradients. Several observations can be made:

- The dynamic flame stands further away from the stagnation point; it has a higher displacement velocity than the static flame.
- The static flame has a higher peak burn rate $\dot{w}_T$, while the dynamic flame shows a wider reaction zone with a longer tail on the products side.
- The temperature of the static flame is higher than that of the dynamic flame throughout the reaction zone, in particular, at the point where $\dot{w}_T$ takes its maximum.
- OH concentrations are almost the same on the reactants side of both flames, but higher on the products side of the dynamic flame.

These distinctions persist throughout the calculation. The temperature at max($\dot{w}_T$) is shown for both static and dynamic flames in Fig. 5; at any given $\dot{Q}$, a larger $d\phi/dt$ produces lower reaction zone temperatures. Clearly, the unsteady change in ϕ_r influences the flame structure significantly, and one cannot explain $\dot{Q}$ enhancement in the dynamic case using the transport lag argument alone.

For the same $\dot{Q}$, lower temperature and reaction rates within the dynamic flame reaction zone are balanced by elevated temperature and OH concentration on the products side; these are the most important features of Fig. 4. Similar to the elevated products-side temperature and radical concentrations introduced externally in the static SuF, these gradients in the wake of the reaction zone maintain higher $\dot{w}_T$ in the tail of the DNaF. The effect is seen even more clearly in Fig. 6, which shows the same two cases of static and dynamic flame structure as Fig. 4. The CO concentration remains significantly higher on the products side of the reaction zone for the dynamic flame than for the static, before dropping to its equilibrium value. This CO tail corresponds to ongoing CO oxidation on the products side of the flame and thus the persistence of heat release. In cases of lower $d\phi_r/dt$, these products-side gradients in radical concentration, CO concentration, and temperature are not observed.

Changes in flame structure resulting from unsteadiness in ϕ were expected, since the dynamic flame processes a mixture with a fuel concentration gradient. Indeed, proceeding from the leading edge
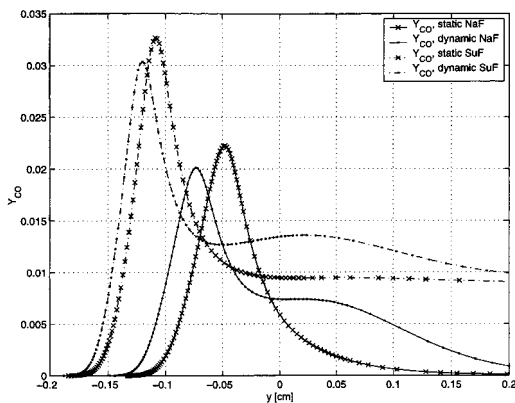
FIG. 6. Static and dynamic CO profiles, for natural flames at $\dot{Q} = 2.96 \times 10^8$ erg/(cm^2 s) and supported flames at $\dot{Q} = 5.24 \times 10^8$ erg/(cm^2 s).

FIG. 8. Comparison of dynamic and static supported flame structure at $\dot{Q} = 5.24 \times 10^8$ erg/(cm^2 s).
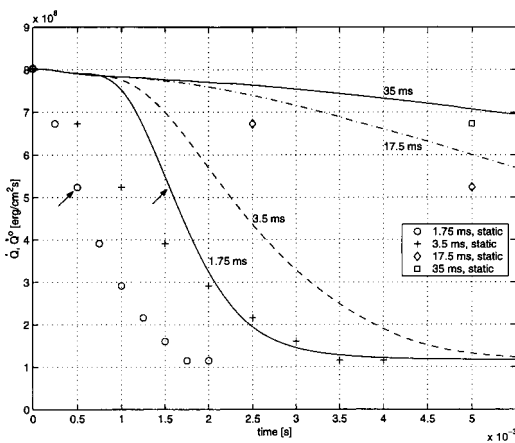

FIG. 7. $\dot{Q}$ versus time for supported flames subject to various $d\phi_r/dt$. Lines are dynamic behavior, while the symbols are static $\dot{Q}$ corresponding to the instantaneously imposed ϕ_r. Arrows denote cases shown in Figs. 6 and 8.

of the flame through the products side, we observed the results of burning at earlier, higher values of ϕ_r—elevated temperature, radical concentration, and CO concentrations. This "history" embedded within the flame structure is a mechanism for the observed "flame inertia" of Fig. 3.

Static versus Dynamic Supported Flames

To refine the results of the previous section, we examined the impact of nonzero $d\phi_r/dt$ while holding ϕ_b constant and equal to 1.0, calling an unsteady flame with this products-side boundary condition a DSuF (for *dynamic supported flame*). The DSuF is interesting for several reasons. First, it eliminates a lingering ambiguity in the structural comparison of
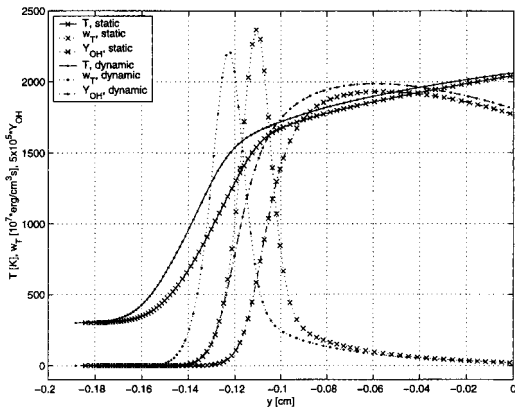
dynamic and static NaFs: static and dynamic NaFs at the same $\dot{Q}$ may not have identical products-side boundary conditions, due to temporal variation in ϕ_b, while static and dynamic SuFs always have identical products streams. The DSuF has physical relevance as well; the burning of a lean pocket in an inhomogeneously mixed reacting flow, or the burning of a premixed flame on a shear layer, are both supported by a reservoir of hot combustion products.

The same linear changes in ϕ_r applied to the DNaF were repeated for the dynamic supported flame. Fig. 7 shows $\dot{Q}$ versus time for the four dynamic cases, along with the corresponding static values. The same results are shown in Fig. 1, plotted versus the instantaneous value of ϕ_r. As with the DNaF, the burning rate for the dynamic flame is always higher than that of the corresponding static case. In comparison with the DNaF, however, we observed the following:

- The time lag was slightly smaller in the DSuF since the flames were thinner.
- The DSuF sustained burning at lower ϕ_r, even when the ϕ gradients were weak, due to the same back support discussed for the static case.
- For fast changes in ϕ_r, the DSuF and DNaF burned at nearly the same rates, while for slower changes, the burning rate of the DSuF was higher than that of the DNaF, again showing the effect of back support.

To examine the role of flame structure in this dynamic response, we again compared static and dynamic flame structures at equal $\dot{Q}$, in Fig. 8. The static supported flame corresponds to $\phi_r = 0.8$, while the dynamic flame corresponds to the 1.75 ms change in ϕ_r, probed 1.55 ms from the start of calculations. As in the comparison for natural flames, the static flame sits closer to the stagnation point,

has a higher peak burn rate, and has a higher temperature throughout the reaction zone. Fig. 5 confirms that larger $d\phi/dt$ produces lower temperatures at the peak of $\dot{w}_T$ for any given $\dot{Q}$. The dynamic flame compensates for a lower peak in $\dot{w}_T$ with a wider reaction zone—a longer tail in $\dot{w}_T$ on the products side. This tail is supported by higher temperature and radical concentrations on the products side, and, referring to Fig. 6, an elevated level of CO, indicating ongoing CO oxidation. Because the dynamic and static supported flames have precisely the same incoming products-stream composition, differences in flame structure to the right of the reaction zone can only be due to unsteadiness in the reactant mixture. The equivalence ratio gradient thus creates internal gradients in the wake of the reaction zone regardless of the products stream boundary condition.

Conclusions

Strained premixed flames propagating through gradients in equivalence ratio in which the length/timescales are comparable with the flame length/timescale exhibit a substantially different response than those burning in uniform streams. They burn faster and can burn into mixtures whose equivalence ratios are lower than those corresponding to flammability limits. The mechanism responsible for these changes is the establishment of spatial gradients in temperature and the accompanying radical concentrations in the wake of the flame—gradients that act as a temporary "heat (and chemical) reservoir" for new incoming reactants. As a result, for the same heat release rate, the reaction zone of a flame burning in a stoichiometric-to-lean equivalence ratio gradient is broader than that of the nominal static flame, with a lower temperature at the peak and a higher radical concentration throughout. These effects are associated with the burning of a mixture that changes its fuel content over the thickness of the flame, here falling to a leaner, more weakly burning mixture as one proceeds from the products side to the reactants side of the flame. In this sense, a strained flame burning a sufficiently steep equivalence ratio gradient generates its own back support, regardless of the actual composition of its products stream.

It is interesting to note—or at this point, speculate—that a lower temperature within the reaction zone resulting from an equivalence ratio gradient would lead to a lower NO_x formation rate for the same overall burning rate. This does not come at the price of higher CO, since the temperature and the radical concentrations remain high for CO oxidation on the products side of the flame. This may help explain why periodic oscillations in equivalence ratio have been observed to reduce overall emissions [19].

REFERENCES

1. Ra, Y., "Laminar Flame Propagation in a Stratified Charge," Ph.D. thesis, Massachusetts Institute of Technology, Cambridge, MA, 1999.
2. Takeda K., Shiozawa, K., Oishi, K., and Inoue T., SAE technical report 851675.
3. Richards, G. A., Janus, M. C., and Robey, E. H., *J. Propul. Power* 15:232–240 (1999).
4. Cohen, J. M., Rey, N. M., Jacobson, C. A. and Anderson, T. J., "Active Control of Combustion Instability in a Liquid-Fueled low NO_x Combustor," paper ASME-98-GT-267, Forty-Third ASME Gas Turbine and Aeroengine Technical Congress, Sweden, 1998.
5. Keller, J. O., "An Experimental Study of Combustion and the Effects of Large Heat Release on a Two Dimensional Turbulent Mixing Layer," Ph.D. thesis, UC Berkeley, Berkeley, CA, 1982.
6. Marzouk, Y. M., "The Effect of Flow and Mixture Inhomogeneity on the Dynamics of Strained Flames," S. M. thesis, Massachusetts Institute of Technology, Cambridge, MA, 1999.
7. Marzouk, Y. M., Najm, H. N., and Ghoniem, A. F., "A Flame Embedding Model for Turbulent Combustion Simulation," paper AIAA-2000-0866, Thirty-Eighth AIAA Aerospace Sciences Meeting, Reno, NV, 10–13 January, 2000.
8. Stahl, G., and Warnatz, J., *Combust. Flame* 85:285–299 (1991).
9. Darabiha, N., *Combust. Sci. Technol.* 86:163–181 (1992).
10. Petrov, C., and Ghoniem, A., *Combust. Flame* 102:401–417 (1995).
11. Egolfopoulos, F. N., *Proc. Combust. Inst.* 25:1365–1373 (1994).
12. M. D. Smooke, ed., *Reduced Kinetic Mechanisms and Asymptotic Approximations for Methane-Air Flames,* Lecture Notes in Physics Series, Springer-Verlag, Berlin, 1990.
13. Smooke, M. D., Puri, I. K., and Seshadri, K., *Proc. Combust. Inst.* 21:1783–1792 (1986).
14. Pernice, M., and Walker, H. F., *SIAM J. Sci. Comput.* 19:302–318 (1998).
15. Eisenstat, S. C., and Walker, H. F., *SIAM J. Optimization* 4:393–422 (1994).
16. Golub, G. H., and van Loan, C. F., *Matrix Computations, 3rd ed.,* Johns Hopkins University Press, Baltimore, 1996.

17. Saad, Y., *Iterative Methods for Sparse Linear Systems,* PWS Publishing, Boston, 1996.
18. Najm, H. N., and Wyckoff, P. S., *Combust. Flame* 110:92 (1997).
19. Poppe, C., Sivasegaram, S., and Whitelaw, J. H., *Control of NO$_x$ Emissions in Confined Flames by Oscillations,* technical report TF/96/09, Imperial College, London, England.

COMMENTS

Robert W. Pitz, Vanderbilt University, USA. These weak limit premixed flames supported by hot products are very interesting because of their relevance to direct-injection spark-ignition engines where such flames are likely to exist. An interesting question is how much additional burning of the weak premixed reactants occurs due to the presence of the hot products stream. In your work, you calculated the integrated heat release rate that is dominated by the hot product stream. Did you compare your integrated heat release values for weak reactants vs. hot products as opposed to hot products vs. air? The difference between these two would give the additional heat release due to burning of the weak premixed mixture from the presence of the hot products stream.

Author's Reply. We do not expect significant heat release to result from air at 300 K impinging on hot products. This is because the lower values of the temperature may quench CO oxidation in the hot products stream. Consider the CO profiles for static flames in Fig. 6: proceeding from the products side to the reaction zone. CO concentrations rise monotonically from their equilibrium values in the burned products mixture, that is, the CO concentration everywhere stays at or above its equilibrium value corresponding to the products stream equivalence ratio. Comparing the integrated heat release rates of supported and natural flames thus provides a meaningful measure of how much additional burning of the "weak" premixed reactants occurs due to the presence of the hot ($\phi\beta = 1.0$) products stream. The higher heat release rate of supported flames burning weak reactants is due to the diffusion of heat and radicals from the products stream.